9. Lipowitz, J., Rabe, J. A., Nguyen, K. T., Orr, L. D. & Androl, R. R. Structure and properties of polymer-derived stoichiometric SiC fiber. *Ceram. Eng. Sci. Proc.* **16,** 55–62 (1995).
10. Bocker, W., Landfermann, H. & Hausner, H. Sintering of alpha silicon carbide with additions of aluminium. *Powder Metall. Int.* **11,** 83–85 (1979).
11. Alliegro, R. A., Coffin, L. B. & Tinklepaugh, J. R. Pressure-sintered silicon carbide. *J. Am. Ceram. Soc.* **39,** 386–389 (1956).
12. Izeki, T. in *Handbook of Corrosion Resistance of Ceramics* (ed. Izeki, T.) 61–67 (Kyoritsu Syuppan, Tokyo, 1985).
13. Takeda, M. & Imai, Y. in *Proc. 7th Symp. on High-Performance Materials for Severe Environments* 227–234 (R&D Inst. of Metals and Composites for Future Industries, Tokyo, 1996).

Acknowledgements. We thank Y. Harada, H. Yamaoka, T. Hisayuki, S. Iwase and T. Fujii for their contributions.

Correspondence and requests for materials should be addressed to T.I. (e-mail: 24613u@ube-ind.co.jp)

DNA-templated assembly and electrode attachment of a conducting silver wire

Erez Braun*, Yoav Eichen†‡, Uri Sivan*‡ & Gdalyahu Ben-Yoseph*‡

** Department of Physics, † Department of Chemistry, ‡ Solid State Institute, Technion-Israel Institute of Technology, Haifa 32000, Israel*

Recent research in the field of nanometre-scale electronics has focused on two fundamental issues: the operating principles of small-scale devices, and schemes that lead to their realization and eventual integration into useful circuits. Experimental studies on molecular[1] to submicrometre[2] quantum dots and on the electrical transport in carbon nanotubes[3–5] have confirmed theoretical predictions[6–8] of an increasing role for charging effects as the device size diminishes. Nevertheless, the construction of nanometre-scale circuits from such devices remains problematic, largely owing to the difficulties of achieving inter-element wiring and electrical interfacing to macroscopic electrodes. The use of molecular recognition processes and the self-assembly of molecules into supramolecular structures[9,10] might help overcome these difficulties. In this context, DNA has the appropriate molecular-recognition[11] and mechanical[12–16] properties, but poor electrical characteristics prevent its direct use in electrical circuits. Here we describe a two-step procedure that may allow the application of DNA to the construction of functional circuits. In our scheme, hybridization of the DNA molecule with surface-bound oligonucleotides is first used to stretch it between two gold electrodes; the DNA molecule is then used as a template for the vectorial growth of a 12 μm long, 100 nm wide conductive silver wire. The experiment confirms that the recognition capabilities of DNA can be exploited for the targeted attachment of functional wires.

The first step in the construction of the silver wire involves the self-assembly of a DNA template connecting two gold electrodes 12–16 μm apart (see Fig. 1 for an outline of the procedure). First, 12-base oligonucleotides, derivatized with a disulphide group at their 3′ end, are attached to the electrodes through sulphur–gold interactions. The electrodes are each marked with specific but different oligonucleotide sequences. A connection is then made by hybridizing two distant surface-bound oligonucleotides with a 16 μm long and fluorescently labelled λ-DNA that contains two 12-base sticky ends, where each of the ends is complementary to one of the two different sequences attached to the gold electrodes. Hybridization on both ends is facilitated by covering the electrodes with an aqueous solution containing the λ-DNA and inducing a flow perpendicular to the electrodes, thereby stretching the λ-DNA molecules in the flow direction (other stretching methods can be used; for application of an electric field, see ref. 17). The flow is terminated when a single DNA bridge is observed by fluorescence microscopy (see Fig. 2), usually after a few minutes. Curving of the DNA bridge under a flow parallel to the electrodes shows it to be attached solely to the electrodes. The method does not guarantee a single DNA bridge. However, *in situ* video microscopy and imaging of the resulting silver wire by atomic force microscopy (AFM; see below) reveal a silver bridge only in places where DNA was previously fluorescently imaged. We also tried stretching the DNA between two electrodes in the reverse order, performing hybridization and ligation of the disulphide-derivatized oligonucleotides to the long DNA molecule before it was applied to the sample (see Methods section). The binding of the derivatized λ-DNA in this case was again aided by an induced perpendicular flow. Both methods work equally well.

To instill electrical functionality, silver metal is vectorially deposited along the DNA molecule. The three-step chemical deposition process (see Fig. 1 and Methods) is based on selective localization of silver ions along the DNA through Ag^+/Na^+ ion-exchange[18] and formation of complexes between the silver and the DNA bases[19–21]. The Ag^+/Na^+ ion-exchange process is monitored by following the almost instantaneous quenching of the fluorescence signal of the labelled DNA. The ion-exchange process, which is highly selective and restricted to the DNA template only, is terminated when the fluorescence signal drops to 1–5% of its initial value (the quenching is much faster than normal bleaching of the fluorescent dye). The silver ion-exchanged DNA is then reduced to form nanometre-sized metallic silver aggregates bound to the DNA skeleton. These silver aggregates are subsequently further 'developed', much as in the standard photographic procedure, using an acidic solution of hydroquinone and silver ions under low light conditions[22,23]. Such

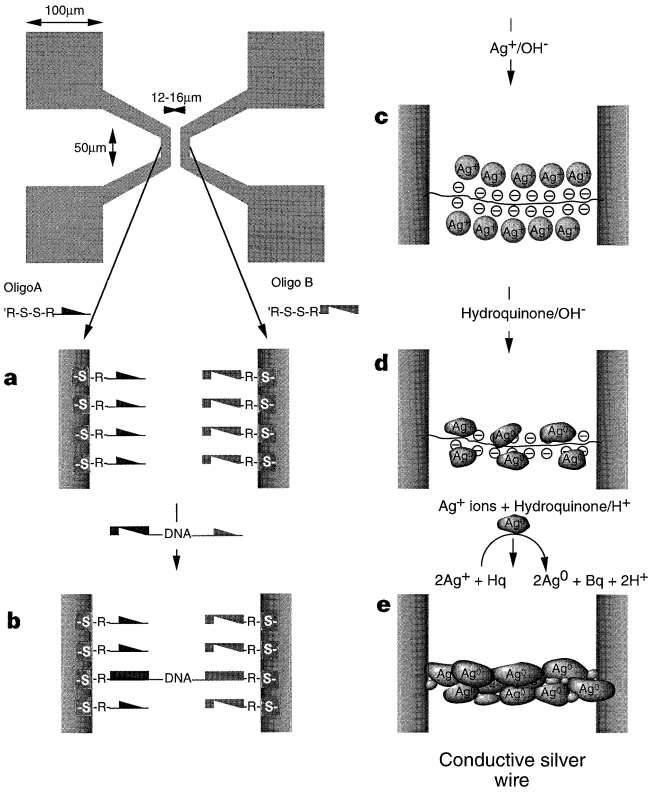

Figure 1 Construction of a silver wire connecting two gold electrodes. The top left image shows the electrode pattern (0.5 × 0.5 mm) used in the experiments. The two 50 μm long, parallel electrodes are connected to four (100 × 100 μm) bonding pads. **a**, Oligonucleotides with two different sequences attached to the electrodes. **b**, λ-DNA bridge connecting the two electrodes. **c**, Silver-ion-loaded DNA bridge. **d**, Metallic silver aggregates bound to the DNA skeleton. **e**, Fully developed silver wire. A full description of the preparation steps can be found in the Methods section.

solutions are metastable, and spontaneous metal deposition is normally very slow. However, the silver aggregates on the DNA act as catalysts and significantly accelerate the process. Under the experimental conditions, metal deposition therefore occurs only along the DNA skeleton, leaving the passivated glass practically clean of silver. The silver deposition process is monitored *in situ* by differential interference contrast (DIC) microscopy and terminated when a trace of the metal wire is clearly observable under the microscope. The metal wire follows precisely the previous fluorescence image of the DNA skeleton. The structure, size and conduction properties of the metal wire are reproducible and dictated by the 'developing' conditions.

AFM images of segments of a 100 nm wide, 12 μm long wire connecting the two gold electrodes are presented in Fig. 3. The images are representative for the whole wire. As clearly seen, the wire consists of grains of 30–50 nm diameter deposited along the DNA skeleton. We have also fabricated wires as narrow as 25 nm but AFM imaging showed the silver coating to be discontinuous, with some gaps between silver grains.

Two-terminal electrical measurements were made on the silver wire shown in Fig. 3. The resultant I–V curves, obtained with an apparatus having an internal resistance of $\geqslant 10^{13}\,\Omega$, are displayed in Fig. 4. The curves are highly nonlinear and asymmetric with respect to zero bias. The shape of the curves depends on the voltage scan direction indicated by arrows. Approaching zero voltage from large positive or negative bias, a zero-current plateau develops with differential resistance larger than $10^{13}\,\Omega$. At a higher bias, the wire again becomes conductive with a differential resistance somewhat lower than in the original bias polarity. Repeated measurements of a given wire, in the same scan direction, yield reproducible I–V curves.

The origin of the extremely high resistance at small bias, and of the dependence of the current on the voltage scan direction, are not yet clear. If one invokes the Coulomb blockade phenomenon and the grain charging energy, ~0.1 eV, as inferred from the grain size in the AFM images, the large plateau requires simultaneous charging of a large number of grains in series. It is not clear, however, whether such a mechanism can yield a history-dependent I–V curve. Another source of nonlinearity might be inter-grain boundary resistance due to silver corrosion. The shape of the I–V curve could then be attributed to electrochemical processes in the corrosion barriers.

The length of the zero bias plateau in different wires may vary from a fraction of a volt to roughly 10 V, depending on the silver growth conditions. The solid line in Fig. 4b depicts, for example, the I–V curve of a different wire in which the silver growth on the DNA was more extensive. Compared with the first wire, the plateau was reduced from about 10 V to 0.5 V, and the differential resistance at voltages beyond the plateau was reduced from 30 MΩ to 7 MΩ. By applying voltages higher than about 50 V to the wires that went through extensive silver deposition, the plateau could usually be permanently eliminated to give ohmic behaviour (dashed-dotted line in Fig. 4b).

Each experiment was accompanied by two control measurements to investigate whether either the DNA bridge or the deposited silver on their own could contribute to the observed electrical transport. The two insets in Fig. 4b show the I–V curves obtained for a λ-DNA bridge in the absence of silver deposition (bottom inset) and for a neighbouring device without a DNA bridge that underwent the full silver deposition treatment (top inset). Both control measurements consistently yielded a resistance higher than our measurement capabilities, $10^{13}\,\Omega$. (Note that the current scale in both insets is 100 times smaller than in the main graph.) Our direct d.c. measurements showed the 16 μm long double-stranded DNA to be practically insulating. It is not clear how to compare our measurements with previously published electron-transfer rates obtained from optical measurements on short DNA segments[24–26]. Perfect correlation was found between the appearance of a DNA bridge in the fluorescence image, the formation of a silver wire connecting the

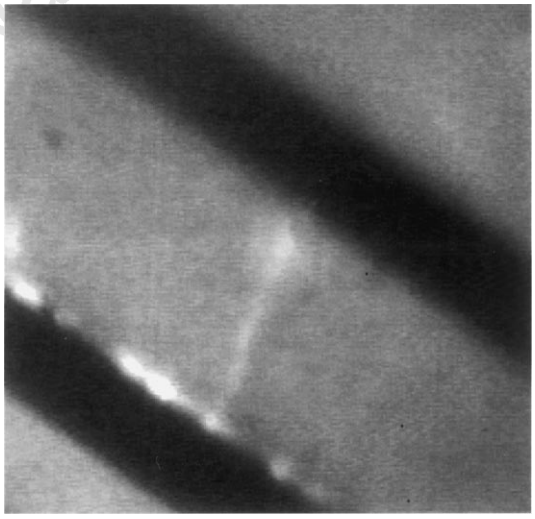

Figure 2 Fluorescence image of the DNA bridge. Fluorescently labelled (Yoyo-1, Molecular Probes, Eugene, Oregon) λ-DNA is stretched between two gold electrodes (dark strips), 16 μm apart. The electrodes are connected to large bonding pads 0.25 mm away.

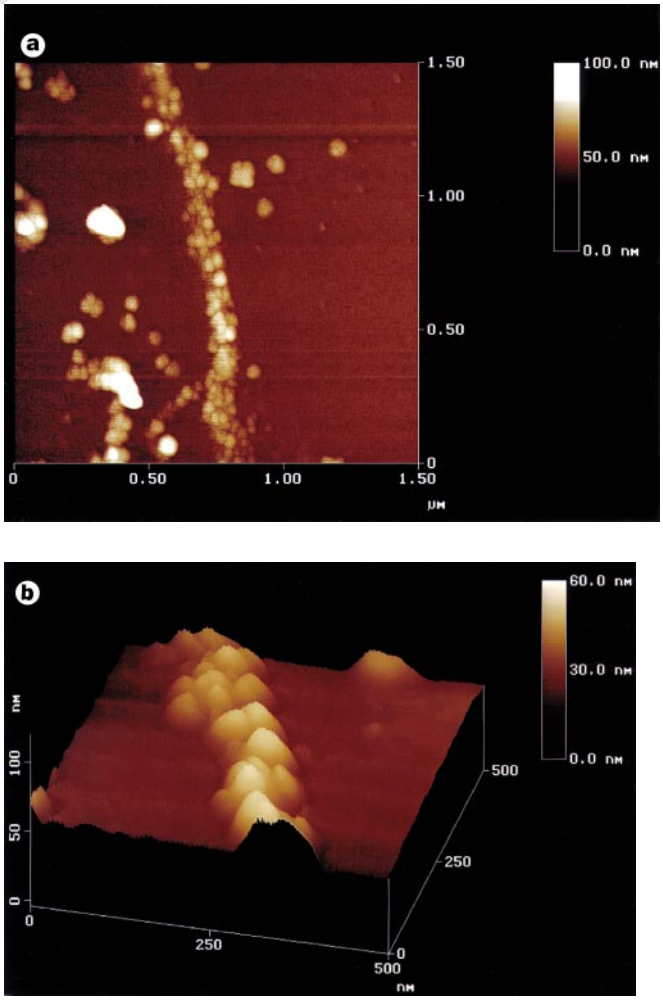

Figure 3 Atomic force microscopy images (Dimension 3000, Digital Instruments) of a silver wire connecting two gold electrodes 12 μm apart. **a**, 1.5 μm; **b**, 0.5 μm field sizes. Note the granular morphology of the conductive wire.

electrodes, and the resulting conduction between the electrodes. These observations, in conjunction with the control experiments, prove that the electric current is carried solely by the silver deposited on the DNA bridge.

The remarkable recognition capabilities of DNA, used in this study to construct a metal wire connecting two electrodes, have also been exploited in other recent studies. The use of DNA has, for example, allowed researchers to organize colloidal particles into macroscopic crystal-like aggregates[27,28] and to dictate the shape and size of semiconductor nanoparticle assemblies[29]. The use of a DNA polyanion as a template for the assembly of electronic materials is not limited to metals. In another study, we have used a DNA template to fabricate a poly-(*p*-phenylene vinylene) (PPV) filament by attaching a positively charged *pre*-PPV polymer to the stretched DNA and subsequently treating it to form a highly photoluminescent PPV wire[30].

The construction of functional nanoscale electronic devices is likely to require self-assembly processes. The present study provides a step towards such developments: we have demonstrated that DNA is a sophisticated substrate for the targeted attachment of a conductive metal wire whose width is well below the minimal dimensions accessible by standard, large-scale microelectronics technology. Even though the hysteric *I*–*V* curves that we observe are interesting, low-resistance, ohmic metal wires are essential for future applications. Such wires might be accessible by making use of different growth conditions, different metal types or post-growth thermal treatments. □

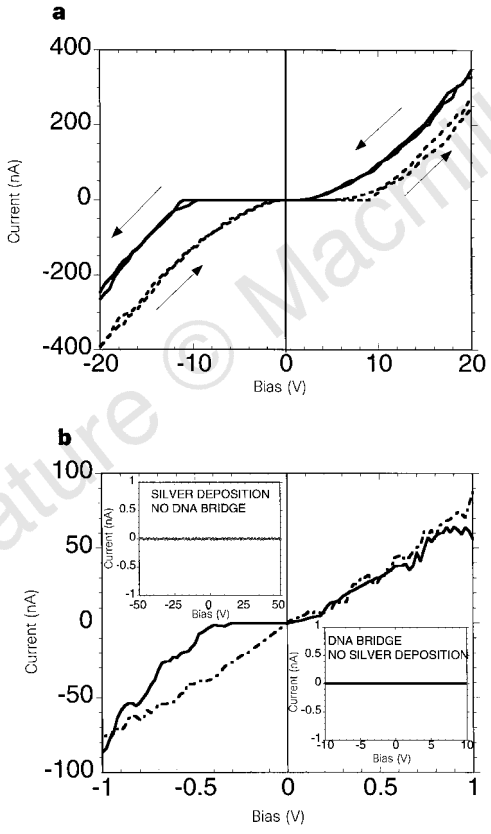

Figure 4 Experimentally observed *I*–*V* curves. **a**, Two terminal *I*–*V* curves of the silver wire shown in Fig. 3. Arrows indicate voltage scan direction. The two curves in each direction present repeated measurements thus demonstrating the stability of a given wire. Note the different asymmetry pertaining to the two scan directions. **b**, *I*–*V* curves of a different silver wire in which the silver growth was more extensive than in **a**. Extensive growth resulted in a narrower current plateau (solid curve), on the order of 0.5 V, and a lower differential resistance (7 MΩ versus 30 MΩ in **a**). By applying 50 V to the wire, the plateau has been permanently eliminated to give an ohmic behaviour (dashed-dotted line), over the whole measurement range. *I*–*V* curves of a DNA bridge with no silver deposition, and silver deposition without a DNA bridge, are depicted in the bottom and top insets, respectively. In both cases, the sample is insulating.

Methods

Sample preparation. A glass coverslip is immersed in fuming nitric acid for 10 min, rinsed with DI water, immersed in a 1M NaOH solution for a further 10 min and rinsed again with DI water. The cleaned glass is dried thoroughly and then passivated against spurious DNA binding by immersion for 12 hours in a 1:5 v/v solution of trimethyl chlorosilane (Sigma) in tetrachloroethane (Sigma). The sample is then rinsed carefully several times with tetrachloroethane and isopropanol and dried thoroughly. Electrodes, 12 μm or 16 μm apart, are defined on the coverslip by standard photolithography and subsequent high vacuum deposition of a 50 nm gold layer on top of a 10 nm titanium adhesion layer. A lift-off process then follows.

Constructing the DNA bridge (see Fig. 1). One gold electrode is wetted with a 10^{-4} μl droplet of an aqueous solution containing 0.2 nM of a 5′-GGGCGGCGACCT-3′-disulphide oligonucleotide (Oligo A) and 10 mM NaCl. Similarly, the other electrode is marked with a solution containing 5′-AGGTCGCCGCCC-3-disulphide oligonucleotides (Oligo B). Both oligonucleotides are synthesized using a 3′-C6-disulphide CPG (Clontech Laboratories, Palo Alto, California). After rinsing, the structure is covered by a 100 μl solution of λ-DNA (0.2 pM, Promega, Madison, Wisconsin) in 10–100 mM NaCl. The λ-DNA has two sticky ends that are complementary to Oligos A and B. A flow perpendicular to the electrodes is induced by micropipette suction of the solution. The flow stretches the λ-DNA molecules perpendicular to the electrodes, leading to their hybridization with Oligos A and B attached to the two electrodes.

Hybridization and ligation before application to the electrodes. The two types of oligonucleotides are phosphorylated at their 5′ ends using T4 polynucleotide kinase (New England Biolabs, Beverly, Massachusetts). The 5′ phosphate of the λ-DNA is removed using Shrimp alkaline phosphatase (Amersham, Arlington Heights, Illinois) to prevent ligation of its complementary sticky ends to form a cyclic DNA. One type of oligonucleotide is then hybridized with the λ-DNA (10^3-fold excess of oligonucleotides) while the solution (sodium phosphate buffer and 1M NaCl, pH = 7) slowly cools down (16 hours) from 75 °C to 4 °C. The hybridization is followed by ligation using T4 ligase (New England Biolabs) at 16 °C for 16 hours. The solution is then filtered (Microcon-100, Amicon, Beverly, Massachusetts) to remove excess free oligonucleotides. The second type of oligonucleotide is then hybridized and ligated with the other sticky end of the λ-DNA using the same procedures.

Silver deposition. Being a polyanion, the DNA bridge is loaded with silver ions by Na^+/Ag^+ ion exchange using a 0.1M $AgNO_3$ basic aqueous solution (ammonium hydroxide, pH = 10.5). The silver ion/DNA complex is reduced using a basic hydroquinone solution (0.05M, ammonium hydroxide, pH = 10.5) to form small metallic silver aggregates bound to the DNA skeleton. The DNA templated wire is 'developed' using an acidic solution (pH = 3.5, citrate buffer) of hydroquinone (0.05M) and silver ions (0.1M) under low light conditions to give a silver wire along the DNA skeleton.

Imaging setup. An inverted microscope (Axiovert 135, Zeiss), equipped with 100× oil-immersed objective, 100-W mercury lamp with filters, image intensifier (C-2400 Hamamatsu) and video processor (Omnex, Imagen Instrumentation), is used for fluorescence imaging of the DNA molecules. The same microscope and objective, with the proper DIC slide, and a 100-W halogen lamp are used for DIC imaging of the silver wire.

Electrical measurements. All electrical measurements were carried out between two bonding pads (see Fig. 1) using a 4145 HP parameter analyser with internal resistance $\geq 10^{13}$ Ω and current resolution of 10 fA.

Received 11 July; accepted 4 November 1997.

1. Porath, D. & Milloh, O. Single electron tunneling and level spectroscopy of isolated C_{60} molecules. *J. Appl. Phys.* **81,** 1–4 (1997).
2. Meirav, U. & Foxman, E. B. Single-electron phenomena in semiconductors. *Semiconductor Sci. Technol.* **11,** 255–284 (1996).
3. Langer, L. *et al.* Quantum transport in a multiwalled carbon nanotube. *Phys. Rev. Lett.* **76,** 479–482 (1996).
4. Tans, S. J. *et al.* Individual single-wall carbon nanotubes as quantum wires. *Nature* **386,** 474–477 (1997).
5. Bockrath, M. *et al.* Single-electron transport in ropes of carbon nanotubes. *Science* **275,** 1922–1925 (1997).

6. Averin, D. V. & Likharev, K. K. in *Mesoscopic Phenomena in Solids* (eds Altshuler, B., Lee, P. & Webb, R.) 173 (Elsevier, Amsterdam, 1991).
7. Grabert, H. & Devoret, M. (eds) *Single Charge Tunneling* (Plenum, New York, 1992).
8. Kastner, M. A. The single-electron transistor. *Rev. Mod. Phys.* **64,** 849–858 (1992).
9. Lehn, J. M. *Supramolecular Chemistry: Concepts and Perspectives* (VCH, Weinheim, 1995).
10. Atwood, J. L. *et al.* (eds) *Comprehensive Supramolecular Chemistry* (Pergamon, Oxford, 1996).
11. Watson, J. D. *et al. Molecular Biology of the Gene* 4th edn (Benjamin Cummings, Menlo Park, 1987).
12. Austin, R. H. *et al.* Stretch genes. *Phys. Today* **50,** 32–38 (1997).
13. Bensimon, D. *et al.* Stretching DNA with a receding meniscus: Experiments and models. *Phys. Rev. Lett.* **74,** 4754–4757 (1995).
14. Bensimon, A. *et al.* Alignment and sensitive detection of DNA by a moving interface. *Science* **265,** 2096–2098 (1994).
15. Wirtz, D. Direct measurement of the transport properties of a single DNA molecule. *Phys. Rev. Lett.* **75,** 2436–2439 (1995).
16. Zimmerman, R. M. & Cox, E. C. DNA stretching on functionalized gold surfaces. *Nucleic Acids Res.* **22,** 492–497 (1994).
17. Schwartz, D. C. & Koval, M. Conformational dynamics of individual DNA molecules during gel electrophoresis. *Nature* **338,** 520–522 (1989).
18. Barton, J. K. in *Bioinorganic Chemistry* (eds Bertini, I. *et al.*) ch. 8 (University Science Books, Mill Valley, 1994).
19. Spiro, T. G. (ed.) *Nucleic Acid–Metal Ion Interactions* (Wiley Interscience, New York, 1980).
20. Marzilli, L. G., Kistenmacher, T. J. & Rossi, M. *J. Am. Chem. Soc.* **99,** 2797–2798 (1977).
21. Eichorn, G. L. (ed.) *Inorganic Biochemistry* Vol. 2, ch. 33–34 (Elsevier, Amsterdam, 1973).
22. Holgate, C. S. *et al.* Immunogold-silver staining: new method of immunostaining with enhanced sensitivity. *Histochem. Cytochem.* **31,** 938–944 (1983).
23. Birrell, G. B. *et al.* Silver-enhanced colloidal gold as a cell surface marker for photoelectron microscopy. *J. Histochem. Cytochem.* **34,** 339–345 (1986).
24. Hall, B. D., Holmlin, R. E. & Barton, J. K. Oxidative DNA damage through long-range electron transfer. *Nature* **382,** 731–735 (1996).
25. Arkin, M. R. *et al.* Rates of DNA-mediated electron transfer between metallointercalators. *Science* **273,** 475–480 (1996).
26. Lewis, F. D. *et al.* Distance-dependent electron transfer in DNA hairpins. *Science* **277,** 673–676 (1997).
27. Mirkin, C. A. *et al.* A DNA-based method for rationally assembling nanoparticles into macroscopic materials. *Nature* **382,** 607–609 (1996).
28. Alivisatos, A. P. *et al.* Organisation of 'nanocrystal molecules' using DNA. *Nature* **382,** 609–611 (1996).
29. Coffer, J. L. *et al.* Dictation of the shape of mesoscale semiconductor nanoparticle assemblies by plasmid DNA. *Appl. Phys. Lett.* **69,** 3851–3853 (1996).
30. Burroughes, J. H. *et al.* Light-emitting diodes based on conjugated polymers. *Nature* **347,** 539–541 (1990).

Acknowledgements. We thank T. Haran, A. Admon, W. Kaplan and S. Lipson for discussions and technical assistance.

Correspondence should be addressed to E.B. (erez@physics.technion.ac.il).

Breakup and conditions for stability of the northern Larsen Ice Shelf, Antarctica

C. S. M. Doake*, H. F. J. Corr*, H. Rott†, P. Skvarca‡ & N. W. Young§

* *British Antarctic Survey, Madingley Road, Cambridge CB3 0ET, UK*
† *Institut für Meteorologie und Geophysik, Universität Innsbruck, Innrain 52, A-6020 Innsbruck, Austria*
‡ *Instituto Antártico Argentino, Cerrito 1248, 1010 Buenos Aires, Argentina*
§ *Antarctic CRC and Australian Antarctic Division, GPO Box 252-80 Hobart, Tasmania 7001, Australia*

The breakup of ice shelves has been widely regarded as an indicator of climate change[1], with observations around the Antarctic Peninsula having shown a pattern of gradual retreat, associated with regional atmospheric warming and increased summer melt and fracturing processes[2–9]. The rapid collapse of the northernmost section of the Larsen Ice Shelf (Larsen A), over a few days in January 1995, indicated that, after retreat beyond a critical limit, ice shelves may disintegrate rapidly. Here we use a finite-element numerical model that treats ice as a continuum without fracture[10] to examine the breakup history[2] between 1986 and 1997 of the two northern sections of Larsen Ice Shelf (Larsen A and Larsen B), from which we establish stability criteria for ice shelves. Analysis of various ice-shelf configurations reveals characteristic patterns in the strain rates near the ice front which we use to describe the stability of the ice shelf. On Larsen A, only the initial and final ice-front configurations show a stable pattern. Larsen B at present exhibits a stable pattern, but if the ice front were to retreat by a further few kilometres, it too is likely to enter an irreversible retreat phase.

Our finite-element model is based on one described by MacAyeal and Thomas[11] that was used to analyse strain-rate patterns on the Filchner Ronne Ice Shelf[12]. A similar model has been used by C. Hulbe (available on the World-Wide Web at http://student-www.uchicago.edu/users/chulbe/science/larsen/larsen.html) to examine the stability of the geometry of the Larsen Ice Shelf after the iceberg calving in 1995. We used the model in a time-independent (diagnostic) mode in which the only input data required are ice thickness and grounding-line velocity. Ice thickness data (Fig. 1) were taken from a mixture of airborne radar ice thickness measurements (made in 1995–96) and surface elevation data from satellite altimetry. Velocities measured in the interior of the ice shelf are too sparse to be used for constraining the ice viscosity through control methods[13]. Measurements that are available[7,14] are used as checks to ensure that modelled velocities conform to realistic values. Except for a softening at the nodes around the margin to one-quarter stiffness, the ice stiffness was constant everywhere, which is equivalent to assuming a uniform depth averaged temperature throughout the ice shelf. Thus the model is of a homogeneous ice shelf and ignores the complexity present in the crevasses and rifts.

We analysed each ice-shelf configuration for its instantaneous strain-rate pattern. We hypothesized that characteristic patterns will emerge that can be associated with the known history and behaviour of the ice shelf. These findings are then used to predict the likely behaviour of Larsen B, at present the northernmost ice-shelf section, under its present circumstances. We assume that a 'stable' ice-front position, although possibly experiencing retreat, is capable of readvancing, but that an 'unstable' position is likely to undergo irreversible retreat. The process of (re)formation of ice shelves is probably very different from their disintegration, with timescales estimated to be of the order of centuries. The complex processes of fracturing and rifting of the ice shelf in response to the flow field and external climatic forcing, although important to the retreat, are poorly known and are not included in our model. We believe the indicators derived from the characteristic patterns are robust under these simplifications. Thus we do not attempt to predict the rate of ice-front retreat or where or when calving will take place, but do indicate the possible consequences if it were to happen.

Dates for the ice-front positions analysed are shown in Fig. 2. The earliest dates used, 1986–89, represent a marginally stable situation for Larsen A and a stable one for Larsen B[6]. The rapid changes taking place on Larsen A, especially around January 1995 when a catastrophic collapse occurred[6], means that several positions were analysed that were close together in time. For Larsen B, only two ice-front positions have been analysed, one for the 'stable' situation before the iceberg calving, also in January 1995, and the other the position in March 1997. There has been continual retreat along most of the ice front since the iceberg calving event, at a rate of a few kilometres per year, with no sign that the trend is about to cease or be reversed[7].

Preliminary model runs using the 1986–89 ice-front positions were carried out using several ice viscosities to find a fit to the observed velocities. The velocities on Larsen B were measured over a two-year period, 1994–96, and so cover a number of ice-front configurations. There was no attempt to find the best fit to the velocities, just a reasonable match, because of the paucity of velocity data and the approximation of uniform viscosity. The chosen viscosity value was used for all ice-front positions. Model runs performed with ice up to 15% thinner near the ice front to test the sensitivity to thickness showed the amplitude of the strain rates there decreased by up to 50% but without any significant change in the pattern. One implication is that ice shelves are more sensitive to climate change through fracture than through thinning.

Model results show that there are large changes in the Larsen A